Multiwavelength Thulium-Doped Fiber Laser Using a Micro Fiber-Optic Fabry–Perot Interferometer
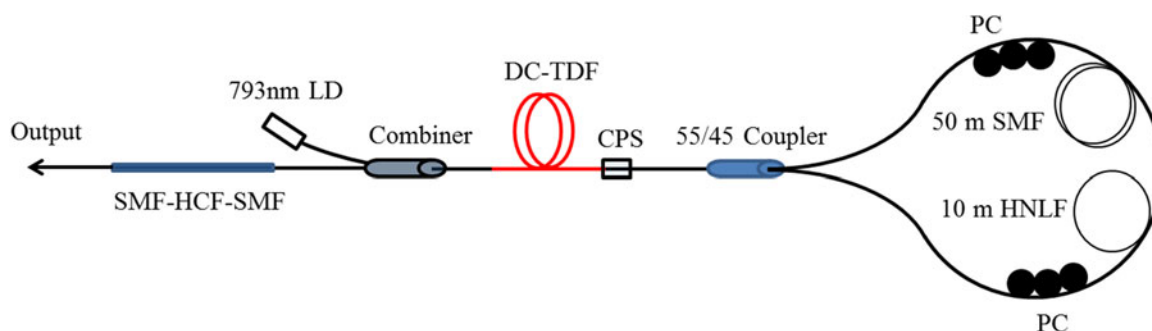
Meng Wang
Yijian Huang
Li Yu
Zongpeng Song
Dezhi Liang
Shuangchen Ruan

Multiwavelength Thulium-Doped Fiber Laser Using a Micro Fiber-Optic Fabry–Perot Interferometer

Meng Wang,[1] **Yijian Huang,**[2] **Li Yu,**[1] **Zongpeng Song,**[1] **Dezhi Liang,**[1] **and Shuangchen Ruan** ⓘ [1]

[1]Shenzhen Key Laboratory of Laser Engineering, Guangdong Provincial Key Laboratory of Micro/Nano Optomechatronics Engineering, College of Optoelectronic Engineering, Shenzhen University, Shenzhen 518060, China
[2]Key Laboratory of Optoelectronic Devices and System of Ministry of Education, College of Optoelectronic Engineering, Shenzhen University, Shenzhen 518060, China

Abstract: A compact, all-fiberized multiwavelength thulium-doped fiber laser based on a micro fiber-optic Fabry–Perot interferometer (FPI) and a nonlinear optical loop mirror (NOLM) has been demonstrated. The FPI with a free spectral range of ∼26 nm was used as an effective wavelength selective filter, which was constructed by splicing a ∼71.4-μm long air-filled hollow-core fiber with single-mode fibers at both ends. An NOLM, served as an amplitude equalizer, was used for stabilizing multiwavelength laser operation. Besides switchable single-wavelength operations (1948.00 and 1972.24 nm), stable dual-wavelength operations (1948.02/1974.25 and 1974.16/1975.30 nm) and triwavelength operation (1947.94/1973.03/1974.14 nm) have been obtained. The optical signal-to-noise ratio of each emission laser line is larger than ∼47 dB.

Index Terms: Multi-wavelength, Tm-doped fiber laser, fiber-optic Fabry-Perot interferometer, nonlinear optical loop mirror.

1. Introduction

Multi-Wavelength fiber lasers have attracted a lot of interest due to their potential applications in wavelength-division-multiplexed (WDM) systems, optical microwave photonic systems, and fiber sensors [1]–[6]. Since the operation wavelength region of thulium-doped fiber laser (TDFL) is ∼1.9 to 2.1 μm, which corresponds to the atmospheric transmission window and the characteristic absorption lines of liquid water and some greenhouse gases, the multi-wavelength TDFLs will have advantages in applications, such as free-space optical communications and gas sensing systems [7], [8].

Till now, many different kinds of filters have been designed for multi-wavelength laser generation, such as Fabry-Perot filter [9]–[11], Mach–Zehnder interferometer [12]–[14], Bragg gratings [15], [16], Spatial mode beating filter [17], [18], Sagnac loop filter [19], and Lyot birefringent filter [20]. Meanwhile, to obtain the stable multi-wavelength laser operation at room temperature, various approaches, including polarization hole burning [21], [22], four-wave mixing [23]–[25], stimulated

Brillouin scattering [26], [27], nonlinear optical loop mirror (NOLM) [28]–[30], and nonlinear amplifier loop mirror (NALM) [31] have been proposed and demonstrated to alleviate the strong mode competition caused by homogeneous gain broadening in rare-earth ions doped fiber. However, we noted that most of the previously reported works were focused on multi-wavelength erbium-doped fiber lasers which operate at 1.5 μm band, and the comparable case of TDFLs has received relatively scant attention. Recently, as for multi-wavelength TDFLs, Soltanian and the co-workers designed a Mach–Zehnder interferometer based on Photonic Crystal fiber for multi-wavelength laser generation, and stable dual-wavelength operated at 1.85 μm was obtained [32]. Fu and the co-workers reported a dual-wavelength TDFL with emission wavelengths above 2 μm by using cascaded single mode-multimode-single mode fiber structures [33]. A widely tunable multi-wavelength TDFL based on a tunable spatial mode-beating filter and a fiber interferometer has been demonstrated by Han and the co-workers [34]. Relying on the nonlinear effect in the fiber theta cavity, a stable all-fiberized multi-wavelength TDFL based on a multimode interference filter has been reported by Wang and the co-workers [35].

In the past few years, the hollow-core fiber (HCF) has received a certain amount of attention due to its applications in pulse compression [36] and fiber sensing [37], [38]. We noted that a compact fiber-optic Fabry-Perot interferometer (FPI) can be implemented by fusion splicing two sections of fibers at both ends of the HCF [39]. This kind of HCF-based FPI with partial reflection at certain wavelengths can act as an effective wavelength selective filter. Moreover, the corresponding transmission part can function as a laser output mirror, which is available for multi-wavelength laser generation in a compact laser cavity. Meanwhile, the free spectral range (FSR) of the fiber-optic FPI can be controlled by manipulating the length of the HCF or the refractive index of the filled media. Nevertheless, this functional fiber-optic FPI has been only used in fiber sensing up to now, the potential application in multi-wavelength fiber lasers has not been done.

In this paper, based on a 71.4-μm long air-filled HCF, a micro fiber-optic FPI with FSR of ~26 nm was fabricated and first used for multi-wavelength continuous wave laser generation in 2 μm band. An NOLM, which functions as an amplitude equalizer, was used to stabilize the multi-wavelength laser operation, and ensure the uniform power distribution among the emission wavelengths. The multi-wavelength TDFL operated steadily with high optical signal-to-noise ratios (OSNRs) (OSNR of each laser line is larger than ~47 dB) and almost equal peak powers (peak power difference between any two laser lines is less than ~1.5 dB).

2. Fabrication and Characterization of the Fiber-Optic FPI

Fig. 1(a) sketches the basic design of the fiber-optic FPI. It was constructed by a 71.4-μm long air-filled HCF (Polymicro Technologies, TSP050150) fusion spliced with two sections of single-mode fibers (SMFs) at both ends, in which a low finesse fiber-optic FPI is formed based on the Fresnel reflection of the perpendicularly cleaved fiber facets at SMF/HCF and HCF/SMF. The HCF with hollow-core diameter of 50 μm (typical cross section can be seen in Fig. 1(a)) has two mainly functions: 1) it determines the length of the Fabry-Perot cavity; 2) it assures alignment between the both SMFs and works as a package to prevent the inside environment was affected by the outside disturbances. It should note that the alignment between the two SMFs in the splicing processing will directly affect the visibility of the interference spectrum. With the assumption of the same reflectivity R (~4%) at the both fiber facet, and neglecting the transmission loss of the HCF, the reflected light intensity of the fiber-optic FPI can be approximated by [37]:

$$I_r \approx 2I_{in}R\left[1 + \cos\left(\frac{4\pi n_{eff}L}{\lambda} + \varphi_0\right)\right] \tag{1}$$

Where I_{in}, I_r, λ, n_{eff}, L, φ_0 are the incident and reflected light beam intensity, wavelength of the probe light, effective refractive index of the probe light, length of the HCF, and constant phase shift, respectively.
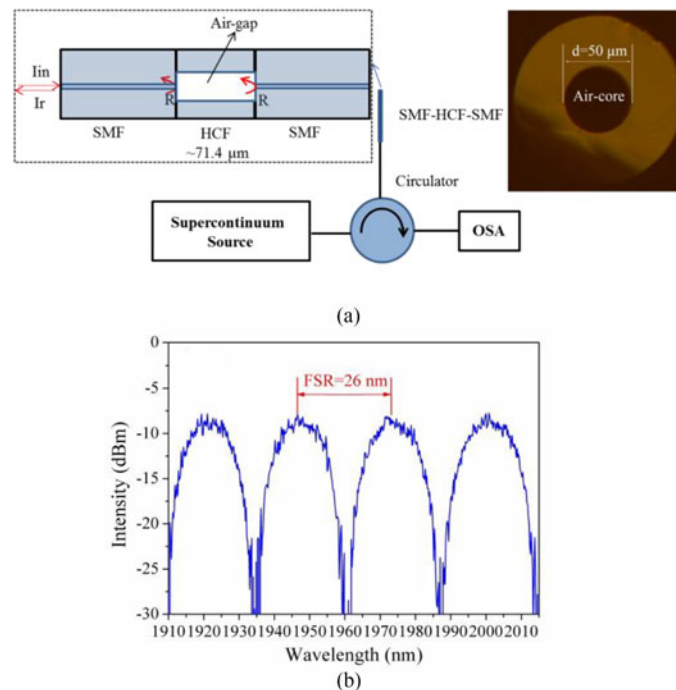
Fig. 1. (a) Schematic diagram of reflection spectrum measurement, (b) reflection spectrum of the fiber optic FPI.
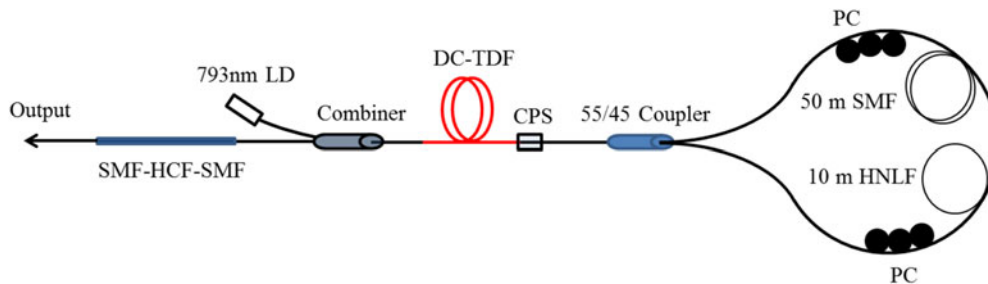

Fig. 2. Schematic configuration of the multi-wavelength TDFL; DC-TDF: double-clad Tm-doped fiber; LD: laser diode; PC: polarization controller; CPS: cladding power stripper; SMF: single mode fiber; HCF: Hollow-core fiber; HNLF: high nonlinear fiber.

The reflection spectrum of the micro fiber-optic FPI was measured by employing the setup shown in Fig. 2(a). A Supercontinuum source (NKT Photonics, SuperK Compact) together with an optical spectrum analyzer (OSA, YOKOGAWA, AQ6375B) were used to measure the reflection spectrum via an optical circulator. At first, we fixed the output power of the Supercontinuum source and directly recorded the output spectrum as A. Then the singlemode-hollow core-singlemode (SMF-HCF-SMF) fiber structure was fusion spliced with the circulator and the output spectrum was recorded as B. Thus, the reflection spectrum is obtained by subtracting A with B, as shown in Fig. 1(b). The reflection peaks have a loss about -8.5 dB, which correspond to the reflectivity of $\sim$14%. By monitoring the transmission power with a continuous wave laser which operates at $\sim$2003 nm (around the reflection peak of the FPI), the insertion loss of $\sim$1.3 dB was mesured. The free spectral range (FSR) of the air-cavity-based FPI is given by:

$$FSR = \frac{\lambda^2}{2nL} \tag{2}$$

Where n is the refractive index of the air. For the 71.4-μm long air-filled hollow-core fiber, the calculated FSR is ~26.6 nm (at ~1950 nm), which agrees well with the measured result shown in Fig. 1(b). The unsmooth reflection spectrum may owe to the weak power fluctuation of the used Supercontinuum source at 2 μm region.

3. Experimental Setup and Principle

The experimental arrangement is schematically shown in Fig. 2. A 105/125 fiber-pigtailed 793 nm multi-mode laser diode (LD) with maximum output power of ~12 W was used for pumping the single mode double-clad Tm-doped fiber (DC-TDF, SM-TDF-10P/130-HE, Nufern) with a length of ~1 m via a $(2+1) \times 1$ pump/signal combiner. The DC-TDF has a core diameter of 10.2 μm and inner cladding diameter of 130 μm with ~3 dB/m cladding absorption at 793 nm. The unabsorbed pump light was effectively stripped by a self-made cladding-power-stripper (CPS). An NOLM was constructed by fusion splicing the fused fiber coupler's both output ports together. The coupler provides a coupler ratio of 45:55 at 2 μm. Two fiber-based polarization controllers were incorporated into the NOLM to strengthen the nonlinear phase difference through the accumulated nonlinear polarization rotation effect. To enhance the nonlinearity of the NOLM, a ~50-m long single mode fiber (SMF) and a ~10-m long high nonlinear fiber (HNLF) were incorporated within. The HNLF exhibits nonlinear coefficient, numerical aperture, core diameter and cladding diameter of 11.68 W^{-1}km^{-1}, 0.35, 3.67 μm, and 120.5 μm, respectively. A SMF-HCF-SMF fiber structure was designed and placed at the other side of the laser cavity, which works as a wavelength selective filter and a laser output mirror at the same time. Thus, an all-fiberized laser cavity was formed.

The NOLM was used for stable multi-wavelength laser operations in 1.5 μm band have been demonstrated [28]–[30], and the mechanism can be easily understood from the transmission characteristic of the NOLM. The transmission of NOLM is given by [40]:

$$T = 1 - 2\alpha(1-\alpha)\{1 + cos(\theta + (1-2\alpha)\varphi)\} \qquad (3)$$

Where α is the splitting ratio of the coupler, θ is the additional phase difference induced by the PCs, and φ is the nonlinear phase shift. As the simulation results in [28], [29], the transmittivity of NOLM can be controlled by adjusting the PCs. When the transmittivity of NOLM increases with the input signal power, the NOLM can act as an artificial saturable absorber. While the PCs are set at a point of where the transmittivity of NOLM degrades as the signal light intensity, the NOLM will function as an amplitude equalizer. The equalizing mechanism of NOLM can alleviate the mode competition in the thulium-doped fiber. Consequently, it can stabilize the multi-wavelength laser oscillations at room temperature, and also ensure the uniform power distribution of the oscillation wavelengths.

4. Experimental Results and Analysis

The pump threshold of the TDFL is ~1.02 W. To obtain the stable laser operation, we fixed the pump power at ~1.40 W. With the careful adjustment of the PCs, stable continuous wave single-wavelength and dual-wavelength laser operations were achieved, as shown from Figs. 3 to 5. Considering the NOLM can generate pulse inside the cavity, we monitored the temporal characteristics of the output laser, and no pulses were observed. Figure 3 shows the single-wavelength laser oscillations at 1948.00 nm and 1974.24 nm respectively, which correspond to the reflection peaks of the fiber-optic FPI. With finely adjusting the PCs, the lasing wavelength can be switched between 1948.00 nm and 1974.24 nm. Both of the laser wavelengths have 3 dB bandwidths of ~0.09 nm and SNRs larger than ~50 dB. Besides the switchable single-wavelength laser emission, stable dual-wavelength laser operations were obtained with proper manipulation of the PCs. Dual-wavelength laser oscillation at 1948.03 nm and 1974.25 nm simultaneously with peak power difference less than ~0.8 dB was shown in Fig. 4(a). The corresponding 3 dB bandwidths and OSNRs of each wavelength are ~0.09 nm, ~0.08 nm and ~49 dB, ~49 dB, respectively. The total output power of the dual-wavelength laser is ~37 mW. By integrating their spectra separately, the individual output
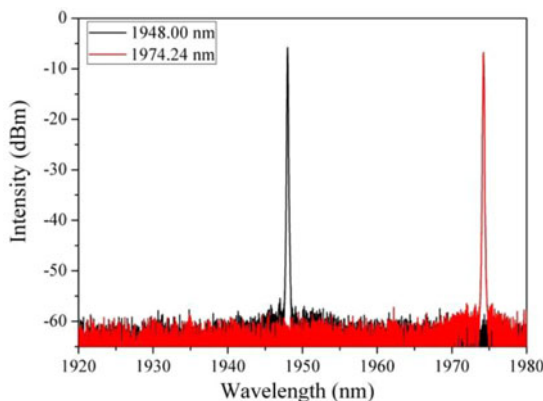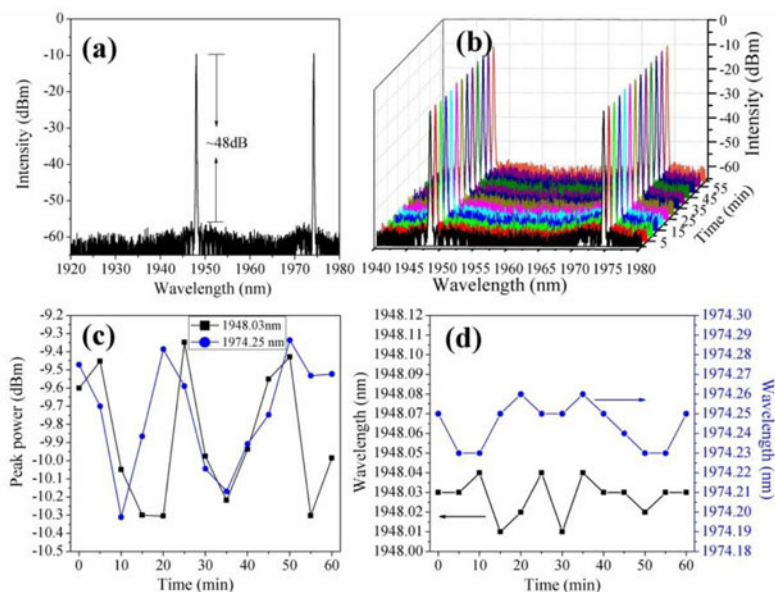
Fig. 3. Switchable single-wavelength laser operation.

Fig. 4. Output characteristics of dual-wavelength laser operation at ~1948.02 nm and ~1974.25 nm. (a) Output spectrum, (b) stability of dual-wavelength laser operation in an hour with interval scanning of every 5 min, (c) peak power fluctuation in an hour, (d) Wavelength fluctuation in an hour.

powers of ~19.4 mW and ~17.6 mW at 1948.00 nm and 1974.24 nm were calculated, respectively. The stability of the generated dual-wavelength has been investigated in an hour with an interval spanning of every five minutes, as shown in Fig. 4(b). The peak power and wavelength fluctuations of each wavelength are in the range of 1 dB and 0.04 nm, as can be seen in Fig. 4(c) and 4(d) respectively, which indicate a good stability of the dual-wavelength laser operation. In the experiment, we noted that another stable dual-wavelength laser operated at 1974.16 nm and 1975.30 nm with peak power difference of less than ~0.5 dB was observed and exhibited in Fig. 5, in which the both lasing wavelengths corresponded to the reflection peak around ~1974 nm. The 3 dB bandwidths, OSNRs and the individual output powers of the two emission wavelengths are ~0.11/0.07 nm, ~48/48 dB and ~24.3/16.7 mW, respectively. We also investigated the spectrum stability of the two emission laser wavelengths, as shown in Fig. 5(b). For better clarity, the peak power and wavelength fluctuations are illustrated in Figs. 5(c) and 5(d), respectively. Both of the wavelengths have peak power fluctuations of less than 0.8 dB and wavelength fluctuations of less than 0.04 nm. The two stable dual-wavelength laser emissions may attribute to the equalizing mechanism of NOLM.
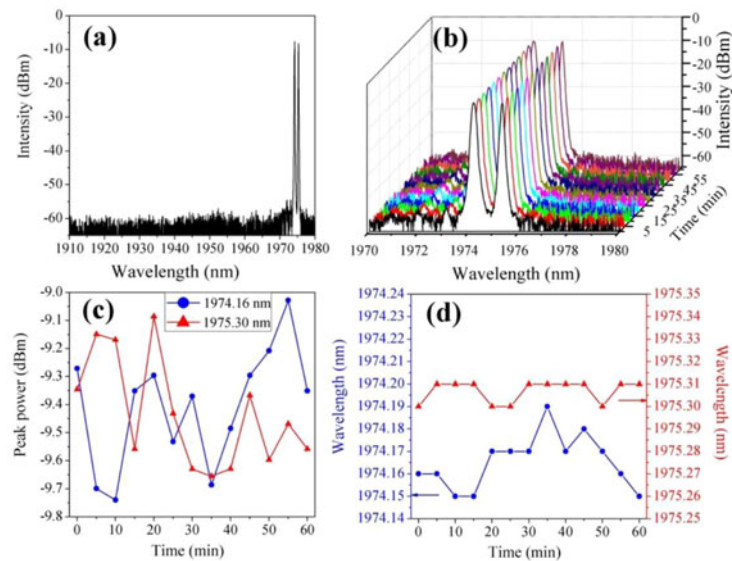
Fig. 5. Output characteristics of dual-wavelength laser operation at ∼1974.16 nm and ∼1975.30 nm. (a) Output spectrum, (b) stability of dual-wavelength laser operation in an hour with interval scanning of every 5 min, (c) peak power fluctuation in an hour, (d) wavelength fluctuation in an hour.

Fig. 6. Output characteristics of three-wavelength laser operation at ∼1947.94 nm ∼1973.03 nm and ∼1974.14 nm. (a) Output spectrum, (b) stability of three-wavelength laser operation in an hour with interval scanning of every 5 min, (c) peak power fluctuation in an hour, (d) wavelength fluctuation in an hour.
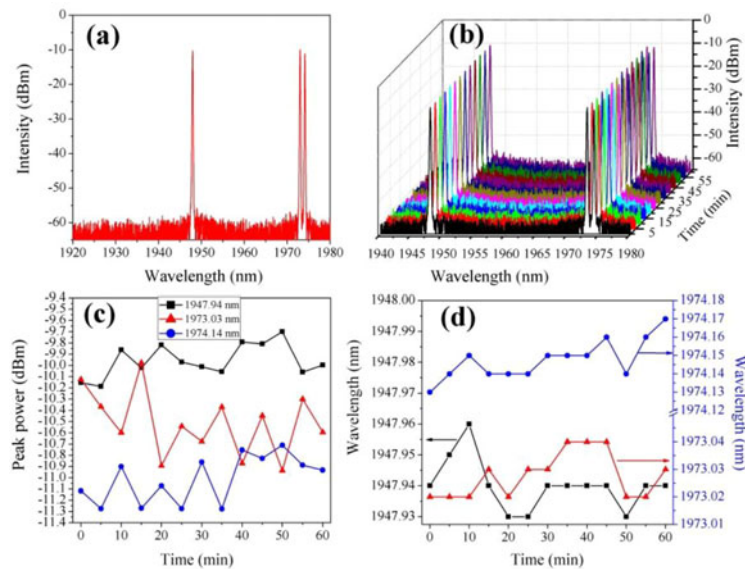
Since the emission wavelengths are located around the reflection peaks of the fiber-optic FPI, which have a minor reflectivity differences. Meanwhile, the equalizing mechanism of NOLM can effectively alleviate the strong mode competition in thulium-doped fiber. Thus a stable dual-wavelength laser operation with uniformed peak power distribution could be obtained.

    After further increasing the pump power from ∼1.40 W to ∼1.69 W and fine-tuning the PCs, tri-wavelength laser operation at 1947.94 nm, 1973.03 nm and 1974.14 nm with 3 dB bandwidths of ∼0.11 nm, 0.1 nm, and 0.1 nm, respectively was achieved and exhibited in Fig. 6(a). The

OSNRs and individual output powers of the three emission wavelengths are ~48/48/47 dB and ~21.3/20.8/15.9 mW, respectively at pump power of ~1.69 W. Also, the spectral stability of the tri-wavelength operation was measured for an hour, as shown in Fig. 6(b). Fig. 6(c) exhibits the peak power fluctuations for each wavelength within an hour, of which the fluctuations at 1947.94 nm, 1973.03 nm and 1974.14 nm are in the range of 0.5 dB, 0.8 dB, and 0.5 dB, respectively. The peak power differences between any two wavelengths are less than ~1.5 dB. Each emission wavelength has wavelength fluctuation of less than 0.04 nm, as plotted in Fig. 6(d). The fluctuations of central wavelength and peak power could be improved by fixing the fibers on the experiment platform to alleviate the disturbance of the environment since the vibration of the fibers will influence the polarization state and the NOLM is polarization sensitive.

5. Conclusion

In summary, we have experimentally demonstrated a compact all-fiberized multi-wavelength TDFL by using a HCF-based fiber-optic FPI together with an NOLM for the first time. The micro fiber-optic FPI plays the roles of wavelength selective filter and laser output mirror at the same time. Switchable single-wavelength operation and stable multi-wavelength operation with nearly identical peak powers were obtained. Each of the emission wavelengths has OSNR of larger than ~47 dB. Our experiment results verified the feasibility of stable multi-wavelength continuous-wave laser generation in TDFL based on a micro HCF-based fiber-optic FPI. This provides a compact and all-fiberized solution to achieve a multi-wavelength lasing in fiber lasers. Moreover, this all-fiberized TDFL has potential applications in tunable multi-wavelength lasers and optical fiber sensing by controlling the filled media in HCF.

References

[1] E. H. Oehler, S. C. Zeller, K. J. Weingarten, and U. Keller, "Broad multiwavelength source with 50 GHz channel spacing for wavelength division multiplexing applications in the telecom C band," *Opt. Lett.*, vol. 33, no. 18, pp. 2158–2160, Sep. 2008.

[2] M. Wang, C. Chen, Q. Li, K. Huang, and H. Chen, "Photonic generation of tunable microwave signal using a passively Q-switched dual-wavelength fiber laser," *Microw. Opt. Technol. Lett.*, vol. 57, no. 1, pp. 166–168, Jan. 2015.

[3] L. Xia, P. Shum, and T. Cheng, "Photonic generation of microwave signals using a dual-transmission-band FBG filter with controllable wavelength spacing," *Appl. Phys. B*, vol. 86, no. 1, pp. 61–64, Jan. 2007.

[4] M. R. K. Soltanian, I. S. Amiri, S. E. Alavi, and H. Ahmad, "Dual-wavelength erbium-doped fiber laser to generate terahertz radiation using photonic crystal fiber," *J. Lightw. Technol.*, vol. 33, no. 24, pp. 5038–5046, Oct. 2015.

[5] S. E. Alavi, M. R. K. Soltanian, I. S. Amiri, M. Khalily, A. S. M. Supa'At, and H. Ahmad, "Towards 5G: A photonic based millimeter wave signal generation for applying in 5G access fronthaul," *Sci. Rep.*, vol. 6, Jan. 2016, Art. no. 19891.

[6] Y. G. Han, T. V. A. Tran, S. H. Kim, and S. B. Lee, "Multi-wavelength Raman fiber laser based long-distance remote sensor for simultaneous measurement of strain and temperature," *Opt. Lett.*, vol. 30, no. 11, pp. 1282–1284, Jun. 2005.

[7] U. N. Singh *et al.*, "Advances in high-energy solid-state 2-micron laser transmitter development for ground and airborne wind and CO_2 measurements," *Proc. SPIE*, vol. 7832, Nov. 2010, Art. no. 783202.

[8] G. Ehret, C. Kiemle, M. Wirth, A. Amediek, A. Fix, and S. Houweling, "Space-borne remote sensing of CO_2, CH_4, and N_2O by integrated path differential absorption lidar: a sensitivity analysis," *Appl. Phys. B*, vol. 90, nos. 3/4, 593–608, Mar. 2008.

[9] C. H. Yeh, C. W. Chow, Y. F. Wu, F. Y. Shih, C. H. Wang, and S. Chi, "Multiwavelength erbium-doped fiber ring laser employing Fabry-Perot etalon," *Opt. Fiber Technol.*, vol. 15, no. 4, pp. 344–347, Aug. 2009.

[10] J. M. Estudillo-Ayala *et al.*, "Multi-wavelength fiber laser based on a fiber Fabry–Perot interferometer," *Appl. Phys. B*, vol. 121, no. 4, 407–412, Dec. 2015.

[11] D. Jauregui-Vazquez, R. Rojas-Laguna, J. M. Estudillo-Ayala, J. C. Hernandez-Garcia, Y. Lopez-Dieguez, and J. M. Sierra-Hernandez, "A multi-wavelength erbium-doped fiber ring laser using an intrinsic Fabry–Perot interferometer," *Laser Phys.*, vol. 26, no. 10, Sep. 2016, Art. no. 105105.

[12] S. Wang, P. Lu, S. Zhao, D. Liu, W. Yang, and J. Zhang, "2-μm switchable dual-wavelength fiber laser with cascaded filter structure based on dual-channel Mach-Zehnder interferometer and spatial mode beating effect," *Appl. Phys. B*, vol. 117, no. 2, pp. 563–569, Nov. 2014.

[13] J. M. Sierrahernandez *et al.*, "A tunable multi-wavelength laser based on a Mach-Zehnder interferometer with photonic crystal fiber," *Laser Phys.*, vol. 23, no. 5, Apr. 2013, Art. no. 055105.

[14] J. Gutierrez-Gutierrez *et al.*, "Switchable and multi-wavelength linear fiber laser based on Fabry-Perot and Mach-Zehnder interferometers," *Opt. Commun.*, vol. 374, no. 1, pp. 39–44, Sep. 2016.

[15] W. Peng *et al.*, "1.94 μm switchable dual-wavelength Tm^{3+} fiber laser employing high-birefringence fiber Bragg grating," *Appl. Opt.*, vol. 52, no. 19, pp. 4601–4607, Jul. 2013.

[16] M. Wang, C. Chen, Q. Li, K. Huang, and H. Chen, "Modulated dual-wavelength Er-doped fiber laser based on a semiconductor saturable absorber mirror," *Opt. Fiber Technol.*, vol. 21, pp. 51–54, Jan. 2015.

[17] A. J. Poustie, N. Finlayson, and P. Harper, "Multiwavelength fiber laser using a spatial mode beating filter," *Opt. Lett.*, vol. 19, no. 10, pp. 716–718, May 1994.

[18] P. Zhang, T. Wang, W. Ma, K. Dong, and H. Jiang, "Tunable multiwavelength Tm-doped fiber laser based on the multimode interference effect," *Appl. Opt.*, vol. 54, no. 15, pp. 4667–4671, May 2015.

[19] X. Ma, S. Luo, and D. Chen, "Switchable and tunable thulium doped fiber laser incorporating a sagnac loop mirror," *Appl. Opt.*, vol. 53, no. 20, pp. 4382–4385, Jul. 2014.

[20] S. Liu *et al.*, "Multi-wavelength thulium-doped fiber laser using a fiber-based lyot filter," *IEEE Photon. Technol. Lett.*, vol. 28, no. 8, pp. 864–867, Jan. 2016.

[21] J. Sun, J. Qiu, and D. Huang, "Multiwavelength Erbium-doped fiber lasers exploiting polarization hole burning," *Opt. Commun.*, vol. 182, pp. 193–197, Aug. 2000.

[22] H. Ahmad, M. R. K. Soltanian, C. H. Pua, M. Z. Zulkifli, and S. W. Harun, "Narrow spacing dual-wavelength fiber laser based on polarization dependent loss control," *IEEE Photon. J.*, vol. 5, no. 6, Dec. 2013, Art. no. 1502706.

[23] Z. Luo *et al.*, "Graphene-assisted multiwavelength erbium-doped fiber ring laser," *IEEE Photon. Technol. Lett.*, vol. 23, no. 8, pp. 501–503, Apr. 2011.

[24] H. Ahmad *et al.*, "Highly stable graphene-assisted tunable dual-wavelength erbium-doped fiber laser," *Appl. Opt.*, vol. 52, no. 4, pp. 818–823, Feb. 2013.

[25] Y. G. Han, T. V. Tran, and S. B. Lee, "Wavelength-spacing tunable multiwavelength erbium-doped fiber laser based on four-wave mixing of dispersion-shifted fiber," *Opt. Lett.*, vol. 31, no. 6, pp. 697–699, Mar. 2006.

[26] Z. Zhang, L. Zhan, and Y. Xia, "Tunable self-seeded multiwavelength brillouin-erbium fiber laser with enhanced power efficiency," *Opt. Exp.*, vol. 15, no. 15, pp. 9731–9736, Jul. 2007.

[27] X. Wang, P. Zhou, H. Xiao, and L. Si, "Multiwavelength Brillouin thulium fiber laser," *IEEE Photon. J.*, vol. 6, no. 1, Feb. 2014, Art. no. 1500507.

[28] X. Feng, H. Y. Tam, H. Liu, and P. K. A. Wai, "Multiwavelength Erbium-doped fiber laser employing a nonlinear optical loop mirror," *Opt. Commun.*, vol. 268, no. 2, pp. 278–281, Dec. 2006.

[29] J. Tian, Y. Yao, Y. Sun, X. Yu, and D. Chen, "Multiwavelength Erbium-doped fiber laser employing nonlinear polarization rotation in a symmetric nonlinear optical loop mirror," *Opt. Exp.*, vol. 17, no. 17, pp. 15160–15166, Aug. 2009.

[30] Z. Zhang, K. Xu, J. Wu, X. Hong, and J. Lin, "Multiwavelength figure-of-eight fiber laser with a nonlinear optical loop mirror," *Laser Phys. Lett.*, vol. 5, no. 3, pp. 213–216, Mar. 2008.

[31] W. Peng, F. Yan, Q. Li, S. Liu, T. Feng, and S. Tan, "A 1.97 μm multiwavelength thulium-doped silica fiber laser based on a nonlinear amplifier loop mirror," *Laser Phys. Lett.*, vol. 10, no. 11, 2013, Art. no. 115102.

[32] M. R. K. Soltanian, H. Ahmad, A. Khodaie, I. S. Amiri, M. F. Ismail, and S. W. Harun, "A stable dual-wavelength thulium-doped fiber laser at 1.9 μm using photonic crystal fiber," *Sci. Rep.*, vol. 5, Oct. 2015, Art. no. 14537.

[33] S. Fu *et al.*, "Dual-wavelength fiber laser operating above 2 μm based on cascaded single-mode-multimode-single-mode fiber structures," *Opt. Exp.*, vol. 24, no. 11, pp. 11282–11289, May 2016.

[34] J. Han, J. Zhang, P. Zhang, T. Wang, and W. Ma, "Widely tunable multiwavelength thulium-doped fiber laser using a fiber interferometer and a tunable spatial mode-beating filter," *Appl. Opt.*, vol. 54, no. 12, pp. 3786–3791, Apr. 2015.

[35] M. Wang, J. Zhao, Y. Huang, S. Lin, and S. Ruan, "Isolator-free unidirectional multi-wavelength Tm-doped double-clad fiber laser based on multimode interference effect," *IEEE Photon. J.*, vol. 9, no. 6, Dec. 2017, Art. no. 1506408.

[36] A. K. George, F. Gérôme, J. C. Knight, K. Cook, and W. J. Wadsworth, "Delivery of sub-100fs pulses through 8m of hollow-core fiber using soliton compression," *Opt. Exp.*, vol. 15, no. 12, pp. 7126–7131, Jun. 2007.

[37] F. Yang, Y. Tan, W. Jin, Y. Lin, Y. Qi, and H. L. Ho, "Hollow-core fiber Fabry-Perot photothermal gas sensor," *Opt. Lett.*, vol. 4, no. 13, pp. 3025–3028, Jul. 2016.

[38] C. Liao *et al.*, "Antiresonant reflecting guidance mechanism in hollow-core fiber for gas pressure sensing," *Opt. Exp.*, vol. 24, no. 24, pp. 27890–27898, Nov. 2016.

[39] B. Qi *et al.*, "Novel data processing techniques for dispersive white light interferometer," *Opt. Eng.*, vol. 42, no. 11, pp. 3165–3171, Nov. 2003.

[40] K. Smith, N. J. Doran, and P. G. Wigley, "Pulse shaping, compression, and pedestal suppression employing a nonlinear-optical loop mirror," *Opt. Lett.*, vol. 15, no. 22, pp. 1294–1296, Nov. 1990.